# Scattering of electromagnetic waves from two-dimensional rough surfaces with an impedance approximation

**G. Soriano and M. Saillard**

*Laboratoire d'Optique Electromagnétique, Unité Propre de Recherche de l'Enseignement Supérieur A 6079, Faculté des Sciences de St Jérôme (case 162), Avenue Escadrille Normandie-Niemen, 13397 Marseille Cedex 20, France*

Received February 9, 2000; revised manuscript received August 1, 2000; accepted August 1, 2000

The sparse-matrix–flat-surface iterative approach has been implemented for perfectly conducting surfaces and modified to enhance convergence stability and speed for very rough surfaces. Monte Carlo simulations of backscattering enhancement using a beam decomposition technique are compared with millimeter-wave laboratory experimental data. Strong but finite conductivity for metals or thin skin depth for dielectrics is simulated by an impedance approximation. This gives rise to a nonhypersingular integral equation derived from the magnetic field integral equation. The effect of finite conductivity for a metal at visible wavelengths is shown. © 2001 Optical Society of America

*OCIS code:* 290.5880.

## 1. INTRODUCTION

Recently much work has been devoted to the rigorous solution of scattering by two-dimensional (2-D) randomly rough surfaces, either perfectly conducting[1–3] or dielectric.[4,5] These studies are based on an integral formalism combined with an iterative solver. In some conditions the concept of a perfectly conducting metal is not relevant. To be convinced of this, one may think of the total absorption of light by a metallic grating.[6–8] Therefore, in principle, one should use the dielectric model with complex refractive index. However, when the imaginary part of the index is high, the free-space Green's function decays very rapidly, and so do the kernels of the integral operators involving the associated wave number. In this case it can be easily shown from the Stratton–Chu equations that the integral relationship between the electric and the magnetic tangential fields on the surface can be approximated by a local relation.[9] This approximation, often referred to as an impedance approximation, has been implemented for one-dimensional (1-D) rough surfaces[10,11] but not yet for 2-D ones. Compared with the Stratton–Chu integral equations, it leads to a reduction by a factor of 2 of the number of unknowns. Here a single equation with locally integrable kernels is derived.[12] For numerical implementation, the regularity of the kernels enables us to use the method of moments with piecewise-constant basis functions or point matching. The iterative solver is very close to that described in Ref. 2. It is also based on the concept of interaction radius[13] and has two iteration levels, but the outer level uses a generalized minimal-residual (GMRes) algorithm, found to be more stable than a relaxation algorithm for deep surfaces. To restrict the size of the linear system, we use narrow Gaussian beams as incident waves, which allow the surface currents to decay rapidly. But from a statistical point of view, to get significant results with the Monte Carlo method, each sample must be large compared with the horizontal length that characterizes the surface statistics, that is, the correlation length for single-scale stationary surfaces with rapidly decreasing correlation function. To obey both constraints, the beam simulation method described in Ref. 14 has been generalized, which permits one to synthesize beams of arbitrary size from the superposition of overlapping narrow beams. With this method there is no restriction on the size of the incident beam. To validate our numerical implementation, we have compared it with experimental data[15] for a deep surface with Gaussian statistics, with very good agreement.

## 2. FORMULATION

A rough surface $S$ separates vacuum from a semi-infinite homogeneous medium. This medium, assumed to be nonmagnetic, is characterized by its complex relative permittivity $\epsilon_r$. $S$ is assumed to be twice continuously differentiable, and its unit normal vector $\mathbf{n}$ is directed toward vacuum. The electromagnetic field is time harmonic, and an $\exp(-iwt)$ time dependence is assumed. The free-space Green's function is written $G_{0p,q} = -\exp(ik_0 r)/4\pi r$ in vacuum, with wave number $k_0 = \omega\sqrt{\epsilon_0\mu_0}$, and $G_{p,q} = -\exp(ikr)/4\pi r$ below $S$, with wave number $k = k_0\sqrt{\epsilon_r}$, where $r$ denotes the distance between the two points $p$, $q$. $\mathbf{j} = \mathbf{n} \times \mathbf{H}$ and $\mathbf{m} = \mathbf{n} \times \mathbf{E}$ denote the electric and the magnetic surface currents respectively, unknowns of the Stratton–Chu equations.

Applying the second Green's vector identity to the electric field at a point in vacuum and taking the limit as this point goes onto the surface, we get

$$(\tfrac{1}{2} + M_0)\mathbf{m} + \frac{s}{\omega\epsilon_0}\mathbf{P}_0\mathbf{j} = \mathbf{n} \times \mathbf{E}^{\text{inc}}. \qquad (1)$$

 © 2001 Optical Society of America

With the magnetic field instead of the electric field,

$$(\tfrac{1}{2} + M_0)\mathbf{j} - \frac{i}{\omega\mu_0}P_0\mathbf{m} = \mathbf{n}\times\mathbf{H}^{\text{inc}}, \tag{2}$$

where $\mathbf{E}^{\text{inc}}$ and $\mathbf{H}^{\text{inc}}$ denote the incident field on the surface. Starting from a point located in the lower medium, we get for the electric field

$$(\tfrac{1}{2} - M)\mathbf{m} - \frac{i}{\omega\epsilon_0\epsilon_r}P\mathbf{j} = \mathbf{0} \tag{3}$$

and for the magnetic field

$$(\tfrac{1}{2} - M)\mathbf{j} + \frac{i}{\omega\mu_0}P\mathbf{m} = \mathbf{0}. \tag{4}$$

$M_0$, $M$ and $P_0$, $P$ are the integral operators introduced by Martin and Ola in Ref. 12. Let $\mathbf{c}$ denote a surface current and $p$, $q$ two points on $S$:

$$M\mathbf{c}_p = \mathbf{n}_p \times \text{rot}_p \int_S G_{p,q}\mathbf{c}_q \text{d}S_q\,, \tag{5}$$

$$P\mathbf{c}_p = \mathbf{n}_p \times \text{rot}\,\text{rot}_p \int_S G_{p,q}\mathbf{c}_q \text{d}S_q\,. \tag{6}$$

$M_0$ and $P_0$ have similar expressions but involve the vacuum Green's function $G_{0p,q}$.

Originally, the sparse-matrix–flat-surface iterative approach[2] (SMFSIA) considered the case of a perfectly conducting surface. This leads to a single equation problem, with electrical surface current $\mathbf{j}$ as unknown. Equations (1) and (2) become the electric and the magnetic field integral equations, respectively:

$$\frac{i}{\omega\epsilon_0}P_0\mathbf{j} = \mathbf{n}\times\mathbf{E}^{\text{inc}}, \tag{7}$$

$$(\tfrac{1}{2} + M_0)\mathbf{j} = \mathbf{n}\times\mathbf{H}^{\text{inc}}. \tag{8}$$

Because it does not involve the $P$ operator, the magnetic field integral equation is better suited to SMFSIA. As a matter of fact, integral equations are cast in a vector-matrix form by use of the moments method with piecewise-constant basis functions and delta test functions.[2] This means that unknown currents are not differentiable. On one hand, writing $M$ as

$$M\mathbf{c}_p = -\int_S \mathbf{n}_p \times (\text{grad}_q\, G_{p,q} \times \mathbf{c}_q)\text{d}S_q\,,$$

it appears that near the pole $r = 0$ the kernel of $M$ behaves as the first derivative of the Green's function, i.e., as $1/r^2$. This singularity can be analytically integrated as a Cauchy principal value. On the other hand, since $P$ involves one more differentiation, it is a hypersingular operator, with the kernel behaving as $1/r^3$. A computable expression for $P$ is

$$P\mathbf{c}_p = \int_S \mathbf{n}_p \times (k^2 G_{p,q}\mathbf{c}_q - \text{grad}_q\, G_{p,q}\,\text{div}_q\,\mathbf{c}_q)\text{d}S_q\,,$$

which requires that the divergence of the current be accessible. This is not compatible with piecewise-constant basis functions. Several ways to overcome this impediment already exist: Divergence can be estimated by numerical differentiation or can be set as an extra unknown. The first solution would be inaccurate, and the second is numerically expensive. More subtle is to consider the operator $(P_0 - P)$, which is less singular than $P$. Indeed, the $1/r^3$ singularity of $P$ is independent of the wave number, i.e., is the same for $P_0$ and $P$, and so disappears in $(P_0 - P)$. In addition, $1/r^2$ singularities also cancel, so that $(P_0 - P)$ is even locally integrable. The following expression for the kernel of $P$ can be found in Ref. 16, p. 267.

$$\text{rot}\,\text{rot}_p(G_{p,q}\mathbf{c}_q) = G_{p,q}\left[\left(\frac{3}{r^2} - \frac{3ik}{r} - k^2\right)(c_q\cdot\mathbf{u})\mathbf{u} + \left(-\frac{1}{r^2} + \frac{ik}{r} + k^2\right)\mathbf{c}_q\right],$$

where $\mathbf{u}$ is the unit vector from point $q$ to point $p$. Its series expansion with respect to $r$ is

$$\text{rot}\,\text{rot}_p(G_{p,q}\mathbf{c}_q) = \frac{1}{4\pi}\left\{-\left[\frac{3}{r^3} + \frac{k^2}{2r} + O(r)\right](\mathbf{c}_q\cdot\mathbf{u})\mathbf{u} + \left[-\frac{1}{r^2} - \frac{k^2}{2r} + O(1)\right]\mathbf{c}_q\right\}.$$

Finally, the behavior of $(P_0 - P)$ at $r = 0$ is written as

$$\text{rot}\,\text{rot}_p[(G_{op,q} - G_{p,q})\mathbf{c}_q] = [(\mathbf{c}_q\cdot\mathbf{u})\mathbf{u} + \mathbf{c}_q]\left[\frac{k^2 - k_0^2}{8\pi r} + O(1)\right].$$

The following combination, $[(1) + \epsilon(3)]$ and $[(2) + (4)]$, leads to a system of two coupled integral equations, without any hypersingular kernel, that can be handled by SMFSIA for the general dielectric case:

$$\left(\frac{1+\epsilon_r}{2} + M_0 - \epsilon_r M\right)\mathbf{m} + \frac{i}{\omega\epsilon_0}(P_0 - P)\mathbf{j} = \mathbf{n}\times\mathbf{E}^{\text{inc}}, \tag{9}$$

$$(1 + M_0 - M)\mathbf{j} - \frac{i}{\omega\mu_0}(P_0 - P)\mathbf{m} = \mathbf{n}\times\mathbf{H}^{\text{inc}}. \tag{10}$$

### A. Impedance Approximation

The use of Eqs. (9) and (10) proves difficult for metals with large but finite conductivity or dielectrics with thin skin depth. This kind of problem is specific. First, the magnetic current is not null but remains small compared with the electric current. Then, when the imaginary part of wave number $k$ is large, the Green's function of the lower medium shows a fast decreasing behavior owing to $\exp(ikr)$, so associated operators $M$ and $P$ have short-range action. With a direct application of the moments method, the currents have to be sampled at the skin-depth scale. A prohibitive number of unknowns is necessary to get a reliable result.[17] From this observation comes the idea of an impedance approximation: Integral relationships (3) and (4) between electric and magnetic surface currents can be approximated by a local, impedancelike relationship. Marvin and Celli[9] have expanded

relation (4) as a series with respect to skin depth $d$. They have shown that this relation is local up to the second order:

$$\mathbf{m}_p = Z\mathbf{j}_p + o(d^2),$$

$$\frac{Z}{\eta_0}\mathbf{j}_p = -ik_0 d\,\mathbf{n}_p \times \left\{1 + d\left[\bar{\bar{S}}_p - \frac{\mathrm{tr}(\bar{\bar{S}}_p)}{2}\right]\right\}\mathbf{j}_p. \quad (11)$$

The impedance $Z$ is only a function of the skin depth $d = i/k$ and of the first and second derivatives of the surface profile at point $p$. $\bar{\bar{S}}_p$ denotes the extrinsic curvature tensor, and its trace $\mathrm{tr}(\bar{\bar{S}}_p)$ equals the sum of the surface's main curvatures.

With this impedance approximation, the thin-skin-depth dielectric problem can be solved with a single integral equation, since the magnetic surface current is no longer present:

$$\left[\left(\frac{1+\epsilon_r}{2} + M_0 - \epsilon_r M\right)Z + \frac{i}{\omega\epsilon_0}(P_0 - P)\right]\mathbf{j} = \mathbf{n}\times\mathbf{E}^{\mathrm{inc}}, \quad (12)$$

$$\left[(1 + M_0 - M) - \frac{i}{\omega\mu_0}(P_0 - P)Z\right]\mathbf{j} = \mathbf{n}\times\mathbf{H}^{\mathrm{inc}}. \quad (13)$$

Since the magnetic current is weak, Eq. (13) is written as a modified magnetic field integral equation (MFIE), with an extra corrective term that represents finite conductivity:

$$\underbrace{\left(\frac{1}{2} + M_0\right)\mathbf{j}}_{\text{MFIE}} + \underbrace{\left\{\frac{1}{2} - M - \frac{i}{\omega\mu_0}(P_0 - P)Z\right\}\mathbf{j}}_{\text{Correction for finite conductivity}} = \mathbf{n}\times\mathbf{H}^{\mathrm{inc}}.$$

The impedance approximation leads to resolutions with approximately the same numerical cost as perfectly conducting surfaces: the number of unknowns and matrix size are unchanged, and only the matrix elements are more complicated and thus take longer to compute.

The surface $S$ has the Cartesian equation $z = f(x,y)$, and $f_p, f_p^x, f_p^y, f_p^{xx}, f_p^{xy}, f_p^{yy}$, denote values of $f(x,y)$ and the first and second derivatives at point $p$. The sampled rectangular part of the plane $(xOy)$ is divided into $N$ similar rectangular subdomains. The moments method is applied to integral equation (13) with piecewise-constant basis functions and delta test functions. The unknown complex vector $\bar{X}$, with length $2N$, contains the values of the product of multiplying the $x$ and $y$ components of the electric surface current $\mathbf{j}$ by $\phi = [1 + (f^x)^2 + (f^y)^2]^{1/2}$ at the center of each of the $N$ subdomains. The $z$ component of $\mathbf{j}$ is linked to the $x$ and $y$ components by $\mathbf{n}\cdot\mathbf{j} = 0$:

$$\bar{X} = [\mathbf{j}_{x_1}\phi_1,\ldots, j_{x_N}\phi_N, \mathbf{j}_{y_1}\phi_1,\ldots, \mathbf{j}_{y_N}\phi_N]^{\mathsf{T}}.$$

The right-hand side $\bar{B}$ is similarly created from the incident field on $S$. From each operator $M_0$, $M$, $(P_0 - P)$, and $Z$ arises a complex $2N$ matrix, constituted by four $N$ submatrices. For example, the operator $M$ gives the matrix $\bar{\bar{M}} = \begin{bmatrix}\overline{\overline{M^1}} & \overline{\overline{M^2}} \\ \overline{\overline{M^3}} & \overline{\overline{M^4}}\end{bmatrix}$. Integral equation (13) is transformed into the linear system

$$\left[(1 + \overline{\overline{M_0}} - \bar{\bar{M}}) - \frac{i}{\omega\mu_0}\overline{\overline{(P_0 - P)}}\bar{\bar{Z}}\right]\bar{X} = \bar{B}. \quad (14)$$

An impedance approximation states that the four submatrices of $\bar{\bar{Z}}$ and $\bar{\bar{M}}$ are diagonal and that $P$ has no influence on nondiagonal terms of submatrices of $\overline{\overline{P_0 - P}}$.

The diagonal elements of $\bar{\bar{Z}}$ are expressed as follows:

$$\bar{\bar{Z}}_{ii} = \begin{bmatrix} Z_{ii}^1 & Z_{ii}^2 \\ Z_{ii}^3 & Z_{ii}^4 \end{bmatrix} = \frac{-i\eta_0 k_0 d}{\phi_i}\left\{\left[1 - \frac{d}{2}\mathrm{tr}(\bar{\bar{S}}_i)\right] \times \begin{bmatrix} -f_i^x f_i^y & -1 - (f_i^y)^2 \\ 1 + (f_i^x)^2 & f_i^x f_i^y \end{bmatrix} + d\begin{bmatrix} -f_i^{xy} & -f_i^{yy} \\ f_i^{xx} & f_i^{xy} \end{bmatrix}\right\}, \quad (15)$$

with

$$\mathrm{tr}(\bar{\bar{S}}_i) = (1/\phi_i^3)\{[1 + (f_i^y)^2]f_i^{xx} - 2f_i^x f_i^y f_i^{xy} + [1 + (f_i^x)^2]f_i^{yy}\}$$

evaluated at the center of each subdomain $i = 1,\ldots,N$.

Now, let us consider the matrix $M_0$. Nondiagonal terms are trivially set equal to the product of the value at the subdomain center by the subdomain area $\Delta$:

$$i \neq j,$$

$$\overline{\overline{M_{0ij}}} = \begin{bmatrix} M_{0ij}^1 & M_{0ij}^2 \\ M_{0ij}^3 & M_{0ij}^4 \end{bmatrix} = \frac{ik_0 r_{ij} - 1}{r_{ij}^2} \times G_{0i,j}\begin{bmatrix} f_j^x x_{ij} + f_i^y y_{ij} - z_{ij} & (f_j^y - f_i^y)x_{ij} \\ (f_j^x - f_i^x) - y_{ij} & f_i^x x_{ij} + f_j^y y_{ij} - z_{ij} \end{bmatrix}\Delta, \quad (16)$$

where

$$x_{ij} = x_i - x_j, \quad y_{ij} = y_i - y_j, \quad z_{ij}f_i - f_j,$$
$$r_{ij} = (x_{ij}^2 + y_{ij}^2 + z_{ij}^2)^{1/2}.$$

Diagonal elements are null for submatrices $\overline{\overline{M^2}}$ and $\overline{\overline{M^3}}$ and are equal for submatrices $\overline{\overline{M^1}}$ and $\overline{\overline{M^4}}$:

$$M_{0ii}^1 = M_{0ii}^4 = \frac{1}{8\pi}\left(f_i^{xx}\int\!\!\int_\Delta \frac{x^2\,dx\,dy}{r^3} + 2f_i^{xy}\int\!\!\int_\Delta \frac{xy\,dx\,dy}{r^3} + f_i^{yy}\int\!\!\int_\Delta \frac{y^2\,dx\,dy}{r^3}\right). \quad (17)$$

For this expression, derivatives of order higher than 2 have been neglected, and only leading terms of the series expansion of the Green's function have been considered. Cauchy principal-value integrals can be analytically evaluated if the surface is approximated by its tangential plane at point $i$, i.e., $r = [x^2 + y^2 + (f_i^x x + f_i^y y)^2]^{1/2}$.

$\bar{\bar{M}}$ having diagonal submatrices, diagonal elements are evaluated by analytical integration of the kernel over the entire $xy$ plane. This gives

$$M_{ii}^1 = M_{ii}^4 = -\frac{d}{4}\frac{f_i^{xx} + f_i^{yy}}{\phi_i}, \tag{18}$$

with all other terms of $\bar{\bar{M}}$ being null.

$(P_0 - P)$ is handled globally to avoid hypersingularity. Operator $P$ is considered only for diagonal elements, so nondiagonal elements of $\overline{\overline{P_0 - P}}$ are also set equal to the product of the value at the subdomain center by the subdomain area $\Delta$:

$$\begin{aligned} i \neq j, \qquad \overline{\overline{P_0 - P}}_{ij} = G_{0i,j}\Bigg[&\left(\frac{3}{r_{ij}^4} - \frac{3ik_0}{r_{ij}^3} - \frac{k_0^2}{r_{ij}^2}\right) \\ &\times \left(\overline{\overline{A1_0}} + \frac{\delta_x^2\overline{\overline{A1_x}} + \delta_y^2\overline{\overline{A1_y}}}{12}\right) \\ &+ \left(-\frac{1}{r_{ij}^2} + \frac{ik_0}{r_{ij}} + k_0^2\right)\overline{\overline{A2}}\Bigg]\Delta, \end{aligned} \tag{19}$$

with the following notation:

$$\overline{\overline{A1_0}} = \begin{bmatrix} -T1_0T3_0 & -T2_0T3_0 \\ T1_0T4_0 & T2_0T4_0 \end{bmatrix},$$

$$\overline{\overline{A1_x}} = \begin{bmatrix} -T1_xT3_x & -T2_xT3_x \\ T1_xT4_x & T2_xT4_x \end{bmatrix},$$

$$\overline{\overline{A1_y}} = \begin{bmatrix} -T1_yT3_y & -T2_yT3_y \\ T1_yT4_y & T2_yT4_y \end{bmatrix},$$

$$\overline{\overline{A2}} = \begin{bmatrix} -f_i^yf_j^x & 1 - f_i^yf_j^y \\ 1 + f_i^xf_j^x & f_i^xf_j^y \end{bmatrix},$$

$$\begin{aligned} T1_0 &= x_{ij} + z_{ij}f_j^x, & T1_x &= 1 + (f_j^x)^2 \\ T2_0 &= y_{ij} + z_{ij}f_j^y, & T2_x &= f_j^xf_j^y, \\ T3_0 &= y_{ij} + z_{ij}f_i^y, & T3_x &= f_j^xf_i^y, \\ T4_0 &= x_{ij} + z_{ij}f_i^x, & T4_x &= 1 + f_i^xf_j^x, \end{aligned}$$

$$\begin{aligned} T1_y &= f_j^xf_j^y, \\ T2_y &= 1 + (f_j^y)^2, \\ T3_y &= 1 + f_i^yf_j^y, \\ T4_y &= f_i^xf_j^y. \end{aligned}$$

For diagonal elements, the $1/r$ singular part is integrated analytically over $\Delta$, whereas the regular part is handled numerically. The singular part is

$$\begin{aligned} &\overline{\overline{P_0 - P}}_{ii}^{\,\mathrm{sing}} \\ &= \frac{k^2 - k_0^2}{8\pi}\Bigg\{\phi_i^2\begin{bmatrix} -\iint_\Delta \frac{xy\,dx\,dy}{r^3} & \iint_\Delta \frac{x^2dx\,dy}{r^3} \\ -\iint_\Delta \frac{y^2dx\,dy}{r^3} & \iint_\Delta \frac{xy\,dx\,dy}{r^3} \end{bmatrix} \\ &\quad + 2\begin{bmatrix} -f_i^xf_i^y & -(1 + (f_i^y)^2) \\ 1 + (f_i^x)^2 & f_i^xf_i^y \end{bmatrix}\iint_\Delta \frac{dx\,dy}{r}\Bigg\}, \end{aligned} \tag{20}$$

and the regular part is

$$\begin{aligned} &\overline{\overline{P_0 - P}}_{ii}^{\,\mathrm{reg}} \\ &= \iint_\Delta\Bigg\{G1\phi_i^2\begin{bmatrix} -xy & x^2 \\ -y^2 & xy \end{bmatrix} \\ &\quad + G3\begin{bmatrix} -f_i^xf_i^y & -(1 + (f_i^y)^2) \\ 1 + (f_i^x)^2 & f_i^xf_i^y \end{bmatrix}\Bigg\}dx\,dy \\ &\quad - \iint_{\mathrm{Supp}(P)\setminus\Delta}\Bigg\{\left(\frac{3}{r^4} - \frac{3ik}{r^3} - \frac{k^2}{r^2}\right)\phi_i^2\begin{bmatrix} -xy & x^2 \\ -y^2 & xy \end{bmatrix} \\ &\quad + \left(-\frac{2}{r^2} + \frac{2ik}{r}\right) \\ &\quad \times \begin{bmatrix} -f_i^xf_i^y & -(1 + (f_i^y)^2) \\ 1 + (f_i^x)^2 & f_i^xf_i^y \end{bmatrix}\Bigg\}\frac{\exp(ikr)}{4\pi r}dx\,dy, \end{aligned} \tag{21}$$

with $\mathrm{Supp}(P)$ the numerical support of the operator and intermediate functions $G1$ and $G3$ derived from the Green's functions:

$$\begin{aligned} G1 &= \left(\frac{3}{r^4} - \frac{3ik_0}{r^3} - \frac{k_0^2}{r^2}\right)\frac{\exp(ik_0r)}{4\pi r} \\ &\quad - \left(\frac{3}{r^4} - \frac{3ik}{r^3} - \frac{k^2}{r^2}\right)\frac{\exp(ikr)}{4\pi r} - \frac{k^2 - k_0^2}{8\pi r}, \\ G3 &= \left(-\frac{2}{r^2} - \frac{2ik_0}{r}\right)\frac{\exp(ik_0r)}{4\pi r} \\ &\quad - \left(-\frac{2}{r^2} + \frac{2ik}{r}\right)\frac{\exp(ikr)}{4\pi r} - \frac{k^2 - k_0^2}{4\pi r}. \end{aligned}$$

### B. Sparse-Matrix–Flat-Surface Preconditioned GMRes: a Modified SMFSIA

Because discretized integral equations lead, for 2-D surfaces, to huge linear systems that cannot be solved with classical methods on standard computers, Pak *et al.* designed the Sparse-Matrix–Flat-Surface Iterative Approach[2] (SMFSIA). As explained previously, the first step in the SMFSIA is the moment method. Then when

we consider the matrices of linear system (14), the terms of most importance are those involving strong interactions, linking neighboring subdomains. Matrix terms with a horizontal distance $\rho_{ij} = (x_{ij}^2 + y_{ij}^2)^{1/2}$ shorter than a chosen neighborhood distance $r_d$ constitute in SMFSIA the *strong* matrices. With the usual $r_d$ of three wavelengths, strong matrices are between 70% and 90% sparse. For computations, these matrices are stored in RAM, with use of a sparse storage mode (for example row index sparse storage mode). Each long-distance term is divided into two: a flat-surface part and a weak part. The Green's function $G$ that appears in each kernel is translationally invariant only for the specific case of a flat surface. For the general rough surface, the translationally invariant part $G_{\mathrm{FS}}$ of $G$ gives rise to the *flat-surface* matrices. These matrices are combinations of block Toeplitz matrices, and so, following a rather intricate procedure,[18] flat-surface-matrix vector products can be computed quickly by 2-D fast Fourier transforms. Another advantage of block Toeplitz matrices is that only one row or one column of storage is needed, and it can be done in RAM. The remainder of strong and flat-surface matrices makes *weak* matrices. These dense, propertyless matrices are not put into RAM. They either are stored on hard disk or evaluated whenever needed:

$$\overline{\overline{\mathrm{Matrix}}} = \underbrace{\overline{\overline{\mathrm{Strong}}}}_{\rho_{ij}<r_d} + \underbrace{\overline{\overline{\mathrm{Flat\text{-}Surface}}}}_{G_{\mathrm{FS}}} + \overline{\overline{\mathrm{Weak}}}. \tag{22}$$

This decomposition allows an exact resolution of the system, with the help of a scheme using two nested iterative methods. In the original SMFSIA, the solution of

$$\overline{\overline{\mathrm{Matrix}}}\,\bar{X} = \bar{B} \tag{23}$$

is seen as the limit of a sequence of solutions of approximate problems,

$$(\overline{\overline{\mathrm{Strong}}} + \overline{\overline{\mathrm{Flat\text{-}Surface}}})\bar{X}_n = \bar{B}_n, \qquad n > 1, \tag{24}$$

with a sequence of right-hand sides,

$$\bar{B}_{n+1} = \bar{B} - \overline{\overline{\mathrm{Weak}}}\,\bar{X}_n, \qquad \bar{B}_1 = \bar{B}. \tag{25}$$

The iteration is stopped when the numerical criterion

$$\|\bar{B} - \overline{\overline{\mathrm{Matrix}}}\,\bar{X}_n\|_2 \leqslant \epsilon\|\bar{B}\|_2 \tag{26}$$

is fulfilled. Approximate problems are solved by a gradient method suited to general complex matrices: the Bi-Conjugate Gradient Stabilized algorithm (BiCGStab), each approximate problem having its own stopping criterion. Experience has shown that it is very efficient for our kind of problem.[19] Relaxation/BiCGStab is the original configuration. The BiCGStab algorithm is fast because it uses the two matrices that are stored in RAM and that have fast matrix-vector products. And even if the right-hand sides take long to generate because of weak-matrix use, relaxation requires very few iterations (typically between five and ten, once again depending on $r_d$). From there comes the efficiency of the SMFSIA. We have successfully implemented this configuration for a large class of roughness, where approximate methods are no longer accurate, but we were unable to reproduce the comparison of Monte Carlo simulations with the experimental data published in Ref. 15. These results concern surfaces with Gaussian height distribution and Gaussian correlation function, the rms height $h$ being one wavelength and the correlation length equal to two wavelengths. For very rough surfaces, relaxation too often fails to converge. We have therefore replaced relaxation by a more advanced and sturdy method: the Generalized Minimal Residual (GMRes) method.

First, let us reconsider the use of flat-surface matrices. Flat-surface matrices have been introduced in the case of a scalar theory with a Dirichlet boundary condition.[20] $G_{\mathrm{FS}}$ is the zeroth-order term of the series expansion of $G$ with respect to ratio $z_{ij}/\rho_{ij}$. Using flat-surface matrices, we get $O(\overline{\overline{\mathrm{Weak}}}\,\bar{x}) = O(k_0 h^2/r_d)$, and flat surface improves convergence for rough surfaces when $h \ll (r_d/k_0)^{1/2}$, which is the range of validity for the series expansion. But outside this range, i.e., for $r_d = 3\lambda$ when the rms height is higher than half a wavelength, the number of iterations becomes smaller without consideration of flat-surface matrices. Second, we have chosen GMRes because it can handle non-Hermitian complex matrices with only one matrix–vector product per iteration. The row-index sparse storage mode used in the strong matrix is inefficient for the transpose matrix-vector product; thus it is another advantage of GMRes that it does not require such a product. GMRes is already known as an efficient algorithm for difficult surface-scattering calculations,[21] and this reputation has been confirmed by our trials of other methods. Finally, GMRes is now a standard, well-known method that can be found in most numerical libraries.

Our goal is not to explain here the theory of GMRes but rather to emphasize the differences between the Relaxation and GMRes configurations. In relaxation, the solution of approximate problems does not need high accuracy for first iterations, because it does not influence the final result. Each new approximate solution uses only the previous one, former solutions being forgotten: there is no memory in relaxation. This is an advantage: the BiCGStab stopping criterion can be loosened at the beginning and tightened when the relaxation criterion is close to being achieved. In contrast, GMRes computes at each iteration $n$ a new vector basis that constitutes with the $n-1$ previous vectors the orthonormal basis of iteration $n$ Krylov space, $\mathcal{K}_n$. From this entire basis one can evaluate the solution that minimizes the 2-norm of the residual $\bar{R}_n = \bar{B} - \overline{\overline{\mathrm{Matrix}}}\,\bar{X}_n$ over space $\mathcal{K}_n$. Therefore the same high accuracy is required for every BiCGStab solution. This is the price of convergence.

Another aspect of the GMRes configuration is that it is more than a two-nested-iterative-method scheme. It can be seen as a preconditioned GMRes algorithm. Preconditioning matrix $\overline{\overline{\mathrm{Prec}}}$ is set to the inverse of $\overline{\overline{\mathrm{Strong}}} + \overline{\overline{\mathrm{Flat\text{-}Surface}}}$, or the inverse of $\overline{\overline{\mathrm{Strong}}}$ if $h \geqslant (r_d/k_0)^{1/2}$ so, that linear system (23) becomes

$$\overline{\overline{\mathrm{Prec}}}\,\overline{\overline{\mathrm{Matrix}}}\,\bar{X} = \overline{\overline{\mathrm{Prec}}}\,\bar{B}. \tag{27}$$

Strong and flat-surface matrices bear the most important terms of the complete matrix, so that the product $\overline{\overline{\mathrm{Prec}}}\,\overline{\overline{\mathrm{Matrix}}}$ is close to identity; and as for relaxation,

GMRes succeeds within a few iterations. The preconditioning matrix $\overline{\overline{\mathrm{Prec}}}$ is never computed explicitly, because products $\bar{V} = \overline{\overline{\mathrm{Prec}}}\,\bar{U}$ are solved as linear systems $\overline{\overline{\mathrm{Prec}}}^{-1}\bar{V} = \bar{U}$ by the BiCGStab method.

The GMRes/BiCGStab configuration has a larger field of convergence, with more stability on samples with the same statistical properties. It has its own limitations that, as is true for the original relaxation/BiCGStab configuration, are difficult to define clearly. It should be noted that not only GMRes but also BiCGStab can fail to converge for too-rough surfaces. Another advantage of GMRes, which can be important for future improvements, is multi-incidence computations. This is a field in which direct methods such as LU decomposition are traditionally superior. Once matrix inversion (or LU decomposition) is done, any number of right-hand sides, i.e., any number of incidence angles, can be handled, whereas each incidence is an entire problem for the SMFSIA. Studies have been done on gradient methods that can efficiently solve multi-incidence computations in a global way.[22]

### C. Beam Decomposition and Parallel Computations

Even with the SMFSIA, there is a maximum surface area that can be handled with given numerical facilities: In order to be efficient, the SMFSIA needs the strong matrix to be stored in RAM, and strong-matrix size increases linearly with the surface area for a given discretization and neighborhood distance. Moreover, a large surface takes a prohibitive amount of CPU time, because a weak-matrix-vector product increases quadratically with surface area. In a Monte Carlo simulation, this maximum size may be too small to represent the statistical properties of a random rough surface. Beam decomposition is an elegant way to overcome this difficulty. It was originally developed for 1-D random rough surfaces,[14] but adaptation to 2-D surfaces is straightforward. Beam decomposition is based on the representation of a *large* beam by a weighted sum of shifted *narrow* beams. Each narrow beam is handled as a particular SMFSIA problem. Summing the surface currents from all the narrow beams provides the surface current of the large one. The scattered field is obtained by making this latter current radiate. An alternative approach is to compute the scattered fields from all the narrow beams and to sum them to get the scattered field from the large beam.

The incident large beam $B$ has the following plane-wave decomposition:

$$\mathbf{H}_B^{\mathrm{inc}}(x,y,z) = \iint_{k_x^2+k_y^2\leqslant k^2} h_B^{\mathrm{inc}}(k_x,k_y)\mathbf{p}^{\mathrm{inc}}(k_x,k_y) \times \exp(ik_x x + ik_y y - ik_z z)\mathrm{d}k_x\mathrm{d}k_y, \quad (28)$$

where $h_B^{\mathrm{inc}}$ and $\mathbf{p}^{\mathrm{inc}}$ denote the plane-wave complex amplitude and the polarization unit vector. Narrow beams have similar decomposition:

$$\mathbf{H}_b^{\mathrm{inc}}(x,y,z) = \iint_{k_x^2+k_y^2\leqslant k^2} h_b^{\mathrm{inc}}(k_x,k_y)\mathbf{p}^{\mathrm{inc}}(k_x,k_y) \times \exp(ik_x x + ik_y y - ik_z z)\mathrm{d}k_x\mathrm{d}k_y. \quad (29)$$

The rigorous relationship between large and narrow beams is the continuous sum

$$\mathbf{H}_B^{\mathrm{inc}}(x,y,z) = \iint_{\mathbb{R}^2} u(X,Y)\mathbf{H}_b^{\mathrm{inc}}(x-X,y-Y,z)\mathrm{d}X\mathrm{d}Y. \quad (30)$$

This sum is over real variables $X$ and $Y$ and is weighted by the complex function $u(X,Y)$. Narrow beams are shifted by $X$ along abscissas and $Y$ along ordinates. The function $u(X,Y)$ is identified with the inverse Fourier transform of the ratio $h_B^{\mathrm{inc}}/h_b^{\mathrm{inc}}$, if the inverse Fourier transform exists. Let us consider the specific case of large and narrow beams with Gaussian shape,

$$h_B^{\mathrm{inc}}(k_x,k_y) = h_B^0 \exp\left\{-\frac{1}{2}\left[\left(\frac{k_x-k_x^0}{1/B_x}\right)^2 + \left(\frac{k_y-k_y^0}{1/B_y}\right)^2\right]\right\}, \quad (31)$$

$$h_b^{\mathrm{inc}}(k_x,k_y) = h_b^0 \exp\left\{-\frac{1}{2}\left[\left(\frac{k_x-k_x^0}{1/b_x}\right)^2 + \left(\frac{k_y-k_y^0}{a/b_y}\right)^2\right]\right\}, \quad (32)$$

centered at plane waves with amplitude $h_B^0$ and $h_b^0$ and wave-vector coordinates $k_x^0$ and $k_y^0$. $B_x$, $b_x$ and $B_y$, $b_y$ are the spatial root mean squares of beams along the $x$ and $y$ axes. Since the incident field is exclusively composed of propagating waves, narrow beams cannot be set arbitrarily narrow, in particular at high mean incident angle. So $b_x$ and $b_y$ must be large enough for the Gaussian amplitudes of the plane waves to be weak for the grazing angles and negligible for wave numbers $k_x^2 + k_y^2 \geqslant k^2$. The inverse Fourier transform exists and is written as

$$u(X,Y) = \frac{h_B^0/h_b^0}{2\pi}\frac{\exp(ik_xX + ik_yY)}{(B_x^2-b_x^2)^{1/2}(B_y^2-b_y^2)^{1/2}} \times \exp\left(-\frac{1}{2}\left\{\left(\frac{X}{(B_x^2-b_x^2)^{1/2}}\right)^2 + \left(\frac{Y}{(B_y^2-b_y^2)^{1/2}}\right)^2\right\}\right). \quad (33)$$

In practice, a finite number of narrow beams is considered, so the sum over $X$ and $Y$ is discretized and bounded:

$$\mathbf{H}_B^{\mathrm{inc}}(x,y,z) = \Delta X\Delta Y \sum_{n=-N}^{N_n}\sum_{m=-N_m}^{N_m} u_{nm} \times \mathbf{H}_b^{\mathrm{inc}}(x-n\Delta X, y-m\Delta Y, z), \quad (34)$$

with $u_{nm} = u(n\Delta X, m\Delta Y)$. The rebuilding of the current (or the scattered field) follows the same rule as for the incident field:

$$\mathbf{j}_B(x,y,z) = \Delta X\Delta Y \sum_{n=-N_n}^{N_n}\sum_{m=-N_m}^{N_m} u_{nm} \times \mathbf{j}_b(x-n\Delta X, y-m\Delta Y, z). \quad (35)$$

Numerical experimentation has shown that a good representation of the large beam is achieved with values of $\Delta X$ and $\Delta Y$ between 1.5 and 2.5 times root mean squares $b_x$

and $b_y$. With the narrow beam extending approximately 6 root mean squares, this means an overlapping of two thirds on each axis.

Beam decomposition is naturally well suited to parallel computation. As a matter of fact, after the rough surface is divided and weights for the decomposition are evaluated, each step (computation of the incident field on the surface, building the matrices, solving the system, and computing the scattered field) is completely independent for each narrow beam. Then scattered fields just have to be summed. This scheme is particularly adapted to the distributed-memory parallel environment. We've used the message passing interface (MPI) library to dispatch each narrow beam on a processor. Computing time is almost divided by the number of processors. Results on aluminum surfaces (see Section 3) have been computed with WMPI, the Windows MPI implementation, on a cluster of five PC's.

## 3. RESULTS AND DISCUSSION

The GMRes/BiCGStab configuration has initially been implemented with the MPI beam decomposition in FORTRAN 90 language on a two-Xeon-Pentium-II–450-MHz-processor PC.

We first show a validation of our program by comparing a Monte Carlo simulation of the field scattered by a metallic randomly rough surface with millimeter-wave experiments. In this frequency range, the perfectly conducting model is generally assumed to be accurate. Surfaces have both Gaussian height distribution and Gaussian correlation function, with the following statistical properties: a height root mean square of one wavelength and a correlation radius of two wavelengths. For Gaussian surfaces, empirical rules, based on numerical experiments dealing with 1-D surfaces, say that at least ten correlation lengths must be illuminated for each sample of the Monte Carlo process. Generalizing this rule to the 2-D case, 130 square surfaces have each been illuminated by a beam with $1/e$ width $B_x = B_y = 4$ wavelengths and mean incidence angle 20°. With such a beam, a 26-wavelength side square was sampled, with six points per wavelength. Under these conditions, the number of unknowns is approximately 50,000. To reduce this number, the beams have been decomposed into 25 narrow beams, leading to 14,000 unknowns for each scattering problem, and, since the neighborhood distance is set to 3 wavelengths, the size of the strong-matrix RAM becomes 200 Mo. Average numbers of iterations are 5.3 for BiCGStab (with a restart parameter of 2) and 7.5 for GMRes. Average computing times are 35 min for a narrow beam and 15 h (divided by the number of processors) for a large beam.

It must be noted that for a perfectly conducting surface, the energy balance between the incident and the scattered field has to be satisfied. In our simulations, this balance is not accurately checked. Between 5% and 9% of the incident energy is lost. The stopping criteria of the gradient methods are not to blame. A better accuracy could be obtained with a tighter discretization and by enlarging the sampled part of the surface. But the improvement is slow and its numerical cost is prohibitive. Using more-elaborate test and basis functions could also help.

Figures 1 and 2 show the bistatic coefficient (the scattered field intensity normalized so that total scattered energy equals $4\pi$) in the plane of incidence for Monte Carlo simulation and millimeter-wave experiments. The curves in Fig. 1, with TE incident waves (electric field perpendicular to the plane of incidence), show very good agreement, especially in cross polarization, although oscillations remain despite use of 130 realizations. The backscattering peaks also coincide very well, in both amplitude and width. The main discrepancy comes from large scattering angles in co-polarization. In principle, the scattered intensity should vanish at $\pm 90°$, but the way the surfaces have been sampled here does not allow us to reach such an accuracy. This is more obvious in Fig. 2 in TM polarization (magnetic field perpendicular to the plane of incidence), where even more energy is scattered into grazing directions. But the comparison of the TM–TM co-polarized components requires some other

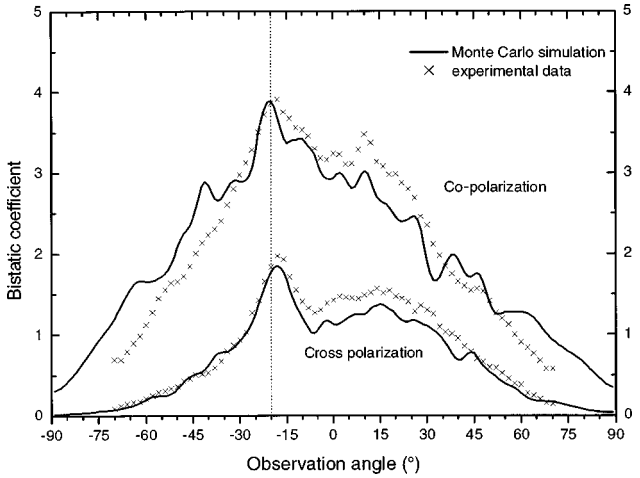


Fig. 1. Comparison of Monte Carlo simulation with experimental data on a perfectly conducting random rough surface: bistatic coefficient in the plane of incidence, TE incidence.

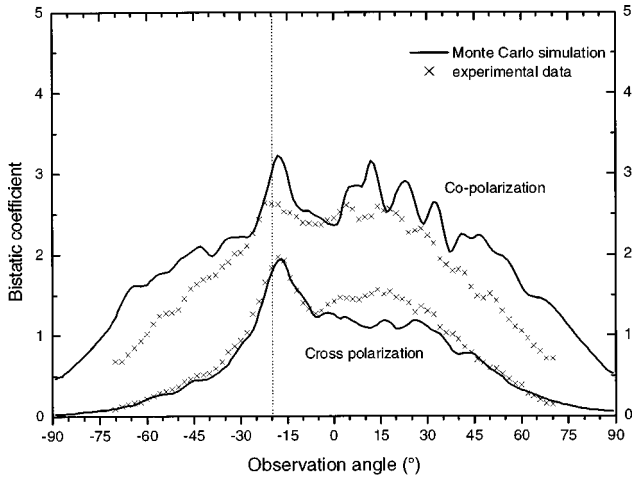


Fig. 2. Comparison of Monte Carlo simulation with experimental data on a perfectly conducting random rough surface: bistatic coefficient in the plane of incidence, TM incidence.

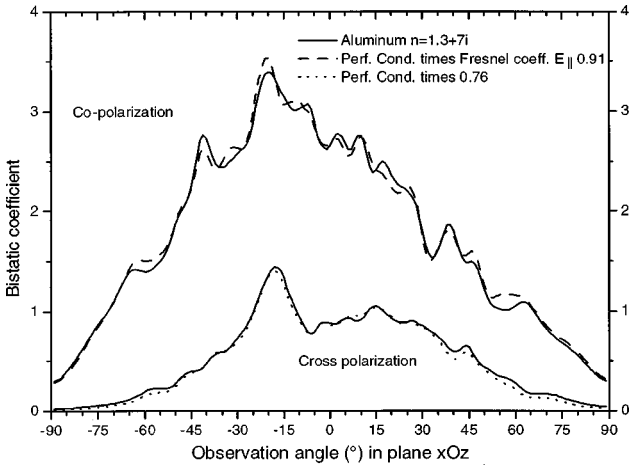


Fig. 3. Comparison between a perfectly conducting and an aluminum random rough surface: bistatic coefficient of Monte Carlo simulation in the plane of incidence, TE incidence.

comments. Indeed, it can be observed that the computed result is always larger than the measured one, even between $-30°$ and $30°$. First, we are convinced that the backscattering peak is missing in the experimental curve. The second point concerns energy balance. Experimental results show much less energy in the plane of incidence in TM than in TE polarization, whereas computations lead to the same amount of energy. This means either that scattering outside the plane of incidence is stronger than predicted by our computations or that there is more absorption in the TM case, which makes the perfectly conducting model questionable. For instance, it is known that in optics this concept is not relevant to the scattering of $p$-polarized waves by 1-D surfaces coated with common metals.

To address this question, we have used the impedance approximation to study the same surface with the same incident beam, but with finite conductivity. We have chosen the optical index of aluminum at 650 nm to be $n = 1.3 + 7.0i$. The imaginary part of this index is large enough to ensure that the supports of operators $M$ and $P$ are narrow compared with the oscillations of the surface current. In Figs. 3 and 4, co-polarized and cross-polarized bistatic coefficients in the plane of incidence are plotted for both perfectly conducting and aluminum surfaces. Even though some oscillations remain, the curves fit very well for TE incidence (Fig. 3), up to a multiplication factor (except possibly at large angles, but the small values of the coefficients are probably not very accurate). For co-polarization the factor equals, as for 1-D surfaces in $s$ polarization, the reflectivity of a flat surface: 0.91; it is 0.76 for cross polarization. Under TM incidence (Fig. 4), the situation is more complicated for co-polarization. Amazingly, the two curves coincide with the ratio 0.90 (also equal to the reflectivity of a flat surface) in the backward direction, and with the ratio 0.76 in the forward direction. As a result, taking the finite conductivity into account drastically reduces the bistatic coefficient between 0° and 90°. This probably explains part of the discrepancy with experimental data discussed above, since the reflectivity of the metallic paint used in the experiments was estimated by the authors to be 0.95. In contrast, the shape of the cross-polarized curves fit very well, again with the ratio 0.76.

It is also interesting to see what happens in the transverse plane (Figs. 5 and 6). This plane is the section of the three-dimensional (3-D) bistatic coefficient plot that is perpendicular to the plane of incidence and that includes the normal emergence. The curves have been symmetrized, according to the isotropy of the surface statistics. The most remarkable result concerns cross polarization. Whatever the incident polarization, the ratio between the bistatic coefficient from the aluminum surface and that from the perfectly conducting one is always very close to 0.76, as in the plane of incidence. A more complete analysis of the data shows that this remains true in all directions. Of course, this number depends on the refractive index and on the geometrical parameters, but we have no explanation for it yet. It must also be noted that the co-polarized curves in Fig. 6 almost coincide up to the reflectivity ratio. Such a behavior has already been observed in the plane of incidence for TE polarization. We conclude that this property holds when the electric field

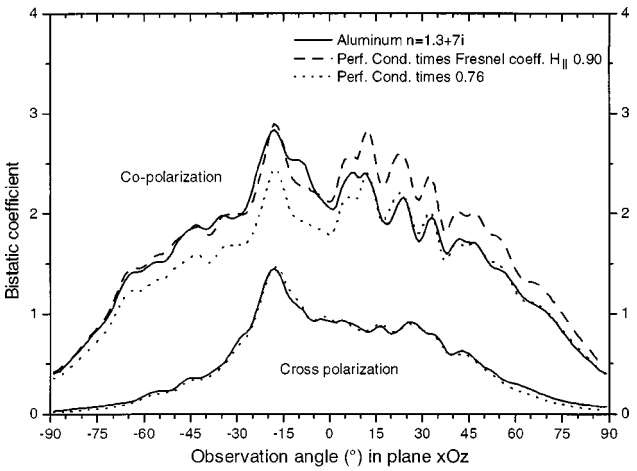


Fig. 4. Comparison between a perfectly conducting and an aluminum random rough surface: bistatic coefficient of Monte Carlo simulation in the plane of incidence, TM incidence.

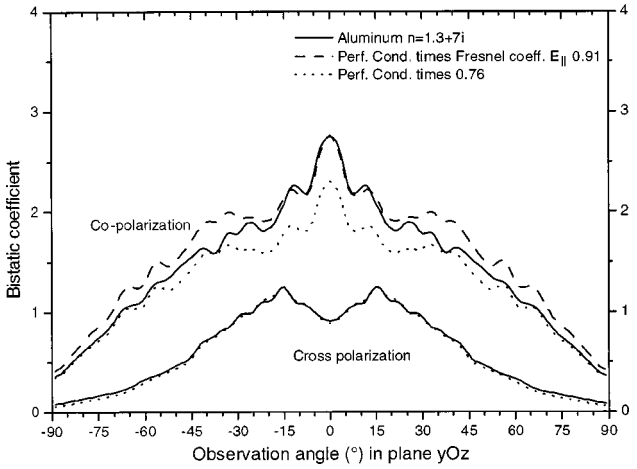


Fig. 5. Comparison between a perfectly conducting and an aluminum random rough surface: bistatic coefficient of Monte Carlo simulation in the transverse plane, TE incidence.

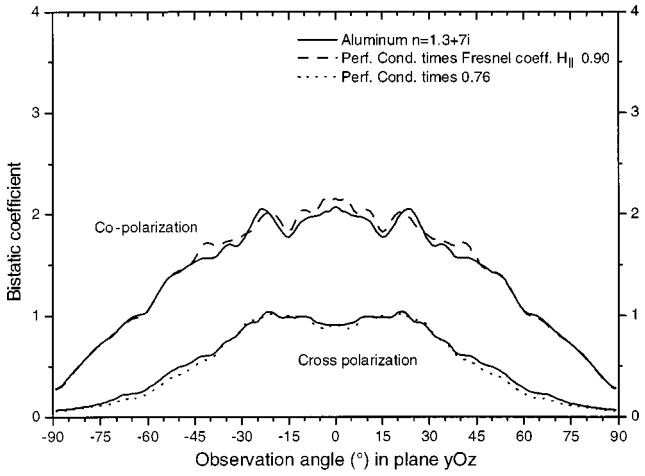


Fig. 6. Comparison between a perfectly conducting and an aluminum random rough surface: bistatic coefficient of Monte Carlo simulation in the transverse plane, TM incidence.

lies in the horizontal plane. Finally, co-polarization in the transverse plane for TE incidence (Fig. 5) exhibits a decreasing ratio from normal (0.91) to grazing (0.76) direction.

To estimate the extra amount of absorption due to surface roughness, we integrated the bistatic coefficient over the whole 3D plot, divided by the same for a perfect conductor, and substracted this ratio from the reflectivity of the metal. We found 6% for TM incidence and 5% for TE incidence. This result points out the main difference from 1-D surfaces under *p* polarization: Here absorption is much lower because energy can escape from the plane of incidence.

At this step, although all these results have to be confirmed by further numerical experiments, it stands out that the behavior of metals such as aluminum in the visible range cannot be simply deduced from that of a perfectly conducting metal. Of course, the bistatic coefficients seem closely related, but except for waves with horizontal electric fields that behave as *s*-polarized waves in 2-D problems, the derivation is not obvious.

## 4. CONCLUSION

An original and efficient implementation of an impedance approximation has been proposed for the rigorous solution of scattering by 2-D rough surfaces. Compared with a more general approach devoted to dielectric media, it allows one to deal accurately with materials with small skin depths at low numerical cost. First, sampling at the skin-depth scale is avoided, and second combining the Stratton–Chu equations cancels the hypersingularity of the kernel of the integral equation. We have solved some problems that occur when the SMFSIA is used for deep surfaces. GMRes is a stable substitute for relaxation when the latter fails to converge, and the use of the flat-surface matrix is no longer fruitful.

Our experience of scattering by 1-D rough surfaces has shown that in *p* polarization, the concept of a perfectly conducting surface is not relevant for predicting the scattering from metallic rough surfaces in optics. Although the results here for isotropic 2-D surfaces are quite different, illuminating with a TM incident wave has clearly pointed out the difference between finite and infinite conductivity. This explains why our simulations with a perfectly conducting model agree very well with experiments in TE polarization and deteriorate in TM polarization.

## 5. ACKNOWLEDGMENTS

The authors thank Région Provence-Alpes-Côte d'Azur and Alcatel Space Industries for supporting G. Soriano's Ph.D. thesis. They also thank the Program National de Télédétection Spatiale and the Office National d'Etudes et de Recherche en Aéronautique for financial support.

Corresponding author G. Soriano's e-mail address is soriano@loe.u-3mrs.fr.

## REFERENCES

1. P. Tran, V. Celli, and A. A. Maradudin, "Electromagnetic scattering from a two-dimensional, randomly rough perfectly conducting surface: iterative methods," J. Opt. Soc. Am. A **11**, 1886–1889 (1994).
2. K. Pak, L. Tsang, C. H. Chan, and J. T. Johnson, "Backscattering enhancement of electromagnetic waves from two-dimensional perfectly conducting random rough surfaces based on Monte Carlo simulations," J. Opt. Soc. Am. A **12**, 2491–2499 (1995).
3. R. L. Wagner, J. Song, and W. C. Chew, "Monte Carlo simulation of electromagnetic scattering from two-dimensional random rough surfaces," IEEE Trans. Antennas Propag. **45**, 235–245 (1997).
4. K. Pak, L. Tsang, and J. T. Johnson, "Numerical simulations and backscattering enhancement of electromagnetic waves from two-dimensional dielectric random rough surfaces with the sparse-matrix canonical grid method," J. Opt. Soc. Am. A **14**, 1515–1529 (1997).
5. V. Jandhyala, B. Shanker, E. Michielssen, and W. C. Chew, "Fast algorithm for the analysis of scattering by dielectric rough surfaces," J. Opt. Soc. Am. A **15**, 1877–1885 (1998).
6. R. W. Wood, "On a remarkable case of uneven distribution of light in a diffraction grating spectrum," Philos. Mag. **4**, 369–402 (1902).
7. D. Maystre, "General study of grating anomalies from electromagnetic surface modes," in *Electromagnetic Surface Modes*, A. D. Boardman ed. (Wiley, New-York, 1982), pp. 661–724.
8. M. C. Hutley and D. Maystre, "The total absorption of light by a diffraction grating," Opt. Commun. **19**, 431–436 (1976).
9. A. M. Marvin, V. Celli, "Relation between the surface impedance and the extinction theorem on a rough surface," Phys. Rev. B **50**, 14546–14553 (1994).
10. M. Saillard and D. Maystre, "Scattering from metallic and dielectric rough surfaces," J. Opt. Soc. Am. A **7**, 982–990 (1990).
11. M. E. Knotts, T. R. Michel, and K. A. O'Donnell, "Comparisons of theory and experiment in light scattering from a randomly rough surface," J. Opt. Soc. Am. A **10**, 928–941 (1993).
12. P. A. Martin and P. Ola, "Boundary integral equations for the scattering of electromagnetic waves by a homogeneous dielectric obstacle," Proc. R. Soc. Edinburgh **123A**, 185–208 (1993).
13. D. Maystre and J. P. Rossi, "Implementation of a rigorous vector theory of speckle for two-dimensional microrough surfaces," J. Opt. Soc. Am. A **3**, 1276–1282 (1986).
14. M. Saillard and D. Maystre, "Scattering from random rough surfaces: a beam simulation method," J. Opt. (Paris) **19**, 173–176 (1988).
15. J. T. Johnson, L. Tsang, R. T. Shin, K. Pak, C. H. Chan, A.

Ishimaru, and Y. Kuga, "Backscattering enhancement of electromagnetic waves from two-dimensional perfectly conducting random rough surfaces: a comparison of Monte Carlo simulations with experimental data," IEEE Trans. Antennas Propag. **44**, 748–756 (1996).
16. R. Petit, *Ondes Electromagnétiques en Radioélectricité et en Optique* (Masson, Paris, 1992).
17. P. Tran and A. A. Maradudin, "The scattering of electromagnetic waves from a randomly rough 2D metallic surface," Opt. Commun. **110**, 269–273 (1994).
18. G. Soriano, "Méthodes numériques pour les problèmes de diffraction à grand nombre de degrés de liberté," Rapport de Diplôme d'Etudes Approfondies (Université d'Aix-Marseille III, Marseille, France, 1996).
19. J. T. Johnson, "Application of numerical models for surface scattering," Ph.D. thesis (Massachusetts Institute of Technology, Cambridge, Mass., 1996).
20. L. Tsang, C. H. Chan, and K. Pak, "Backscattering enhancement of a two-dimensional random rough surface (three-dimensional scattering) based on Monte Carlo simulations," J. Opt. Soc. Am. A **11**, 711–715 (1994).
21. J. C. West and J. M. Sturm, "On iterative approaches for electromagnetic rough-surface scattering problems," IEEE Trans. Antennas Propag. **47**, 1281–1288 (1999).
22. P. Soudais, "Iterative solution of a 3-D scattering problem from arbitrary shaped multidielectric and multiconducting bodies," IEEE Trans. Antennas Propag. **42**, 954–959 (1994).